SSC20-WKIV-07

Integrating Globally Dispersed Calibration in Small Satellites Mission Value

Afreen Siddiqi, Sheila Baber, Olivier L. de Weck

Massachusetts Institute of Technology
77 Massachusetts Avenue, Cambridge, MA 02139, USA
siddiqi@mit.edu

Chris Durell, Brandon Russell, Jeff Holt
Labsphere Inc.
North Sutton, NH 03260, USA
cdurell@labsphere.com

ABSTRACT

The availability of earth observation (EO) data has rapidly increased from small satellite missions, however, there are often important deficiencies in its accuracy due to lack of calibration. If calibration is rigorously used with emerging sensors, there can be important improvements in reducing uncertainty with profound implications in use of remote sensing data for climate modeling, disaster recovery, and other applications. Here, a novel methodology for modeling the value of multi-spacecraft earth observation missions with globally dispersed calibration systems for frequent radiometric calibration of earth imaging sensors is presented. The mission value is quantified with a proxy metric, Effective Data Acquired (EDA), which is the total data returned by the system for regions of interest to data users over the operational life of the EO system. The EDA is adjusted with calibration-related discounting factors determined by the rate at which data accuracy declines and the frequency of re-calibration for each sensor. The method is demonstrated for small spacecraft constellations for earth imaging. The simulated results, for the specific case, show that the adjusted-EDA is reduced by ~18% (from ~2900 TB to ~2400 TB) for a degradation rate of 0.05% over a 60-day time period. Overall, the adjusted-EDA can be used for relative comparisons in trade studies with varying mission design and calibration site and frequency parameters.

INTRODUCTION

Use of small satellite missions is expanding for a variety of Earth Observation (EO) applications. While the availability of data has rapidly increased, there are important challenges in its accuracy and reliable use[1]. Sensor calibration, which is the process of quantitatively determining an instrument's response to known controlled signal inputs[2], is of critical importance for earth observation. Its importance has only grown where new systems now consist of several sensors such as that provided by small spacecraft constellations or multi-platform systems that combine space-based and air-based observation platforms. As all sensors undergo degradation over time (due to mechanical, thermal and electrical effects, space weather and UV exposure), periodic radiometric calibration helps maintain data accuracy and consistency. This becomes vital as new applications of EO require Analysis ready data (ARD), and that is only possible with a common understanding and documentation of traceable calibration and data processing chains.

Historically, calibration for orbiting platforms has relied on a combination of reference sensors (large monolithic spacecraft with on-board calibration hardware), Pseudo-Invariant Calibration Sites (PICS, a few of which are instrumented), and targeted (staffed) vicarious calibration campaigns. These methods have been shown to be capable of achieving a 3% relative uncertainty in best-case execution and have limited frequency opportunities (mean time between calibrations). If calibration opportunities are increased and can be provided to different missions on-demand, there can be important improvements in reducing uncertainty, and thereby affect the accuracy of derived data products. Implications of improved data products can be profound for climate modeling, disaster recovery, and other applications. This is due in part because even small errors in the raw data can be amplified downstream[3].

This paper presents a new methodology for quantitatively modeling the value of multi-spacecraft earth observation missions in which the presence of globally dispersed calibration systems providing

frequent radiometric calibration for earth imaging sensors is explicitly incorporated. A theoretical framework, building on prior work on distributed spacecraft mission value[4], is advanced in which calibration-related adjustment factors are included in quantifying mission value. This method thus provides a systematic basis for determining impact of calibration on value, and for conducting trade studies[5] for in-space (on-orbit observation platforms) and ground-based (calibration sites) elements in system architecture.

In the following sections, a brief literature review and existing research gaps are first discussed. Next, an overview of quantifying value of remote sensing systems, based on proxy metrics of data produced from those systems is provided. In the following section, new conceptual extensions to the metrics are presented that incorporate data degradation and calibration. A summary of an analytical framework is then described that allows for quantifying calibration value for different remote sensing applications. An application case is demonstrated with preliminary results. Lastly, key limitations of the current work and future work are discussed.

LITERATURE REVIEW

With the advent of small spacecraft [6], and an increasing recognition for their role in earth observation and earth science [7,8], it is important to develop new approaches for their data calibration, harmonization, and consistency.

In case of large monolithic spacecraft (such as Landsat 8), sensors are well-designed and calibrated prior to launch, and recalibration is frequently performed during the orbiting mission so that any degradations in instrument function are offset[9]. This is important for maintaining accuracy over the multi-year missions. Studies have found differences of up to 16% for multi-spectral scanner (MSS) systems used in early Landsat missions [10]. In the case of Landsat 8's OLI (Observational Land Imager) instrument, an annual degradation in instrument gain of up to -0.2% was detected in all reflective bands, such that over 7+ years of operation, the calibration errors amount to ~2.3%. The effect of the degradation is to make targets appear darker than they really are over time. For example, in the Blue band, a 30% reflector in 2012 would appear to have a reflectance of 29.6% in 2016 and 29.3% in 2020 [9,11].

While periodic calibrations ensure accuracy in case of large spacecraft, there are no common systems or standards currently in place for calibrating small spacecraft that have moved beyond the realm of design, experimentation, and testing [12]. In some cases, small spacecraft are relying on intercalibration with other larger, on-orbit spacecraft[13]. Data fusion of small spacecraft with data from other sensors (such as Landsat and MODIS) has been used for earth science applications such as estimation of Normalized Difference Vegetation Index (NDVI) and Leaf Area Index (LAI) for studying crop growth and harvesting [14], and evapotranspiration studies [15]. These approaches rely on use of reliable data from large observatories, and are dependent on availability of suitable data for cross-calibration and validation. So far, such applications are emerging, but there are inherent limitations to such intercalibrations. For instance, intercalibration requires consistency of spectral bands, spatial collocation, and consistency of viewing geometry. Additionally, even for an image taken by two different instruments on the same day within a short time interval at nadir view, the radiance at the instruments can be different due to changes in the solar illumination angle, changes in the atmosphere between the time the two measurements are taken, and due to the Bidirectional Reflectance Distribution Function (BRDF) of the target. A change in the solar angle has several important impacts: change in the solar zenith angle alters the incident solar irradiance, and the path and path length through the atmosphere can change. Even for a constant homogeneous atmosphere, the amount of scattering and absorption, and the resulting direct and diffuse irradiance at the surface changes. This can be modeled for known atmospheric conditions, however, atmospheric conditions are usually not known for image pairs when intercalibrations are performed [13].

Here, in this study, a new approach is examined in which the utility of independent, on-ground vicarious calibration systems is assessed. In theory, such calibration systems can provide greater opportunities for calibration and data harmonization and can be customized for particular constellations at desirable temporal frequencies and locations. This paper presents a novel method to evaluate the impact of globally dispersed vicarious calibration systems on the value of small satellite missions.

REMOTE SENSING SYSTEM VALUE BASED ON ACQUIRED DATA

The value of space systems that provide services, such as commercial communications or entertainment, has been traditionally quantified with financial measures such as Net-Present Value (NPV) [16] that accounts for the discounted financial difference of revenue and costs over the service life of a system. However, for Earth observation (EO) systems where the generated data can be used for a variety of applications

that may serve scientific and public use, typical financial approaches are not applicable for quantifying value. To address this issue, a conceptual approach was developed, wherein value of an EO system architecture (consisting of one or more spacecraft), with a specified mission in a particular class of observation objectives, is based on the total quantity (and quality) of data returned over the system lifetime. The following sections describe the approach in detail.

Quantifying remote sensing architecture value

The total useful data returned by the system for regions of interest to data users over the operational life can provide a quantitative proxy measure of the value of the EO system [4].

The extent of data acquisition, over *k*-regions of interest, is measured with an 'effective data acquired' (EDA) metric which is computed as [4]:

$$EDA_k = \sum_{j=1}^{S} \sum_{i=1}^{I_j} Q_{ij}^k \frac{\mu_{ij}^k}{\sigma_{ij}^k} \qquad (1)$$

In Eq. 1, Q_{ij}^k is the quantity of data acquired over region *k* in observation window *i* by spacecraft *j*. The symbols μ and σ are mean and standard deviation respectively of a suitable quality metric of the collected data. For imaging sensors, the quality metric can be the signal-to-noise ratio (SNR), computed as [17]:

$$SNR = \frac{N_e}{N_t} \qquad (2)$$

$$N_e = \frac{L_T A_{gp}}{|R|^2} * \left(\frac{D_{ap}}{2}\right)^2 * \pi * \tau_{op} * T_i * Q_e \qquad (3)$$

$$L_T = L_E + L_S^{uw} \quad (4)$$

$$L_S^{uw} = \frac{L_S^{dw} * \frac{A_{gp}}{|T - P_{sun}|^2} * cos\,(\theta_i^{drv})}{4\pi} \qquad (5)$$

Where N_e, is the Number of Electrons at the Detector, N_t is the Total Number of Noise Electron, A_{gp} is the Observation Ground Pixel Area, L_T is Total Radiance from Target Area, *R* Range Vector from Satellite to Target Ground Point, L_E is Radiance from Earth in direction of Ground Pixel, L_S^{uw} is Upwelling reflected Solar Radiance from Ground Pixel, L_S^{dw} is Downwelling Radiance at Target Observation Ground Pixel.

In this formulation of EDA, it should be noted that Q (data quantity) will be based on how frequently a region of interest comes into view by a particular spacecraft. Thus, the revisit frequency of regions of interest is automatically incorporated in the metric with higher levels of Q.

The EDA from each target region, that may have weight w_k in terms of importance of data from that region, can be combined into a single value as:

$$\sum_{k=1}^{W} w_k EDA_k \qquad (6)$$

This quality-adjusted data quantity measure provides a simple, but useful way to compare different types of architectures (with varying spacecraft, orbital locations, and desired observation requirements geometries) [18]. The metric can be further refined by accounting for data acquired by different spectral bands of a sensing platform. Overall, the EDA can serve as a useful measure for comparing different designs and architectures for earth observation missions trade studies wherein number of spacecraft, orbital parameters, and types of instruments have to be chosen. Conversely, the EDA metric can also be used for relativistic comparisons between deployed and fielded missions where sensors are operating in space.

It is interesting to note that the concept of an 'effective' metric has precedent in other measures used in remote sensing literature. This includes the 'effective resolution element (ERE)' used for quantifying the spatial resolving power, and the 'effective instantaneous field of view (EIFOV)'. The ERE was developed to address deficiencies of the more common measure, Instantaneous field of view (IFOV), which is defined as the area of the ground that is viewed by the instrument from a given altitude at any given instant of time. While the IFOV provides a geometrical definition, it does not take into account the spectral properties of the target. Since remote sensing detects and records radiance of targets, the definition of spatial resolution should account for the way in which the radiance is generated [19]. The ERE was accordingly defined as "the size of an area for which a single radiance value can be assigned with reasonable assurance that the response is within 5% of the value representing the actual relative radiance." [19]. More details on the effective instantaneous field of view (EIFOV) can be found in cited papers [19].

Incorporating time in value of data

The Net Present Value (NPV) is widely used in financial accounting. It incorporates the time value of money in future cash flows (that may be obtained in a project or in a service providing system) as:

$$NPV = [Revenue_0 - Cost_0] + \frac{[Revenue_1 - Cost_1]}{1+r} + \ldots + \frac{[Revenue_n - Cost_n]}{(1+r)^n} \qquad (7a)$$

The revenue and cost in each future time period are discounted, and for the k_{th} future time period, the discount factor is $\frac{1}{(1+r)^k}$, where r is called the discount ratio (or rate).

Equation 7a shows a discrete time representation of the NPV. Its formulation in continuous time is often given as:

$$NPV = \int_{to}^{tf} (revenue - cost) e^{-rt} dt \qquad (7b)$$

wherein the conversion between continuous or discrete representation is based on the general relationship [20]:

$$\int_{t=0}^{\infty} e^{-at} dt = \sum_{t=1}^{\infty} \left(\frac{1}{1+a}\right)^t \qquad (7c)$$

Using the concept of NPV, an analogous measure, *Net Architecture Value* (NAV) of a system, was defined as [4]:

$$V = \int_{t=0}^{n} (DataAcquired \times \omega - cost)\, e^{-rt}\, dt \quad (8a)$$

or in discrete form, it can be represented as:

$$V = \sum_{k=0}^{n} \frac{Data\ Acquired_k \times \omega}{(1+r)^k} - \sum_{k=0}^{n} \frac{Cost_k}{(1+r)^k} \qquad (8b)$$

where $Cost_k$ is monetary cost incurred in period k, Data acquired $_k$ is quantity of data acquired (and provided to users) in period k, ω is a monetizing parameter in dollars per bits, r is a discount ratio, and n is the total number of time periods. Here, the data acquired can be equal or related to EDA described in Eq. 6. For the case of EO systems, the discrete time periods can be daily, weekly, monthly or yearly depending on particular applications and systems.

Integrating calibration in value

The utility of the acquired data is directly related to its accuracy and quality (and for some applications, its timeliness). A sensor's data has highest accuracy at the instant of its calibration, after which a decline occurs over time until the sensor is recalibrated and its accuracy is restored. This temporal decline in accuracy (and thus in its utility or value) can be represented with an additional 'discounting factor'. This would be analogous to how discount rates in financial evaluation combine rates of inflation with premiums for "risk" to get risk-adjusted discount ratios [21].

If the data quality adjustment is represented with an additional factor, r_ε , then Eq. 8a is changed to:

$$V = \int_{t=0}^{n} (DataAcquired \times \omega)\, e^{-(r+r_\varepsilon)\, t} - (cost)\, e^{-rt}\, dt \quad (9a)$$

$$V = \sum_{k=0}^{n} \frac{Data\ Acquired_k \times \omega}{(1+r+r_\varepsilon)^k} - \sum_{k=0}^{n} \frac{Cost_k}{(1+r)^k} \qquad (9b)$$

In this paper, for an initial model, r_ε is formulated as a linear mathematical function related to sensor calibration and calibration frequency. Then, if a fully-calibrated EO sensor initiates operations (with pre-launch and post-launch calibration), then value of r_ε at the initial time is zero. However, with the passage of time, it increases as data quality degrades continuously until the sensor undergoes a recalibration event. If calibration events occur at time instances $t_1 \ldots t_i \ldots t_n$ during operations, then r_ε can be represented as shown in Figure 1.

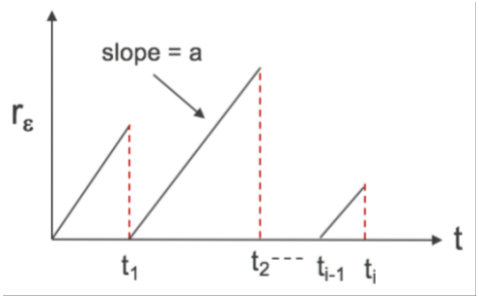

Figure 1: A stylized diagram showing how r_ε, that quantifies data degradation due to loss of sensor calibration, may vary over time with calibration events occurring at time instances t_i. Each calibration event resets this data degradation factor to zero. The calibration events may not be spaced equally in time due to the specifics of the orbital geometry and the location of the calibration site.

The linear formulation is given by:

$$r_\varepsilon = a(t - t_i) \qquad (10)$$

where $t - t_i$ is the time interval elapsed since the last calibration event of the sensor at time instance t_i, and a is a constant parameter representing how fast the sensor calibration loss (or degradation) occurs.

The numerical value of a will be based on empirical data and can use manufacturers' specifications of the sensor. However, it will also need to incorporate effects due to the operational environment such as thermal effects, radiation, and so on that will vary depending on the specific mission and orbital geometry. In this paper, a is assumed to encompass all the combined factors: thermal, optical, sensor response, electronics etc. that collectively lead to degradation, and

is used as an aggregate parameter for studying the impact of periodic calibration.

Adjusted Effective Data Acquired

The value formulation shown in Equation 9 is for a general case for monetary evaluation of costs and benefits. To demonstrate its application, and for simplicity in this paper, it is assumed that ω is unity, the monetary discount ratio r is zero, and costs are not included. Furthermore, Data Acquired is equal to EDA, then Eq. 9 leads to:

$$V = EDA_{adj} = \int_{t=0}^{n} EDA\, e^{-r_\varepsilon t}\, dt \qquad (11a)$$

$$V = EDA_{adj} = \sum_{k=0}^{n} \frac{EDA}{(1+r_\varepsilon)^k} \qquad (11b)$$

Here, the value is thus simply represented with EDA_{adj}, which is the effective data acquired adjusted for any degradation due to loss of calibration. This adjusted metric can be used for systematic analysis and relative comparisons. The following sections describe its use in more detail.

CALIBRATION INTEGRATION VALUE ANALYSIS (CALVIN) FRAMEWORK

A Calibration Integration Value Analysis (CalVIN) simulation framework is being developed for integrated analysis of calibration and value of EO systems (Fig. 2). The tool will allow for computing value and optimizing networks of globally dispersed calibration systems that provide improved and more frequent radiometric services to spacecraft constellations and multi-platform space and air-borne optical sensors. It consists of a set of computational modules that obtain simulations of orbits and coverage and instrument performance, and combine this information with models of data quality degradation and calibration, and system costs and revenue to compute value.

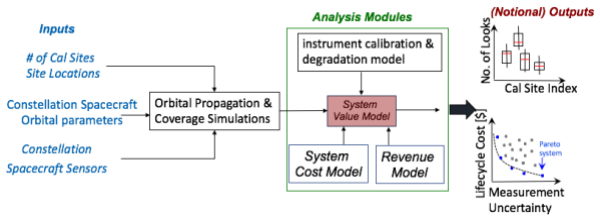

Figure 2: CalVIN consists of modules for computing calibration system costs and value for EO missions.

Overall, CalVIN features a multi-disciplinary integration of models of physics, engineering, and economics for system trade studies. The rest of the paper describes the use of the CalVIN framework that implements the value model presented in the previous sections.

APPLICATION CASE: EARTH IMAGING SMALL SATELLITE CONSTELLATIONS

A number of small spacecraft have been deployed for earth imaging, and there are increasing plans to further grow earth imaging systems in the future[7]. In this work, such systems are used to demonstrate a proof-of-concept of the proposed mission value computation methodology.

Case A: Adjusted EDA for a small satellite constellation

For a first application case, a hypothetical cubesat constellation of 12 spacecraft with passive imaging sensors viewing the continental United States was modeled and simulated. Each spacecraft was assumed to be identical, with a mass of 5 kg, operating at a 450 km altitude in a sun synchronous orbit (SSO). Each (identical) instrument was modeled as a 12-bit imager with detector width d = 7.5 e-6 m, focal length f = 1.14 m, diameter of aperture D_{ap} = 0.091 m, along track FOV = 1.9773$_o$, cross-track FOV = 2.9662$_o$, and a Quantum Efficiency Q_E = 0.5.

The orbital simulations were conducted with the Tradespace Analysis Tool for Constellations (TAT-C)[5,22]. This tool incorporates elements of the General Mission Analysis Tool (GMAT) developed by NASA GSFC, but has several additional capabilities for modeling instrument performance. Some key outputs include SNR, Dynamic Range, Noise-Equivalent-Delta Temperature (NEDT), and Ground Pixel Resolution [23]. Users can also provide information for ground stations (such as a calibration site) within a Region of Interest in order to perform Point of Interest (POI) revisit statistics such as frequency and duration.

Figure 3 shows the results of the orbital simulation for the region of interest (continental US) for a 60-day simulation. The simulation used 818 points of interest (POI) to compute coverage and observation statistics, and the varying frequencies of access by the constellation are shown in Fig. 4. The POI with the highest number of access events, (marked red in Fig. 4), was assumed as the calibration site for the constellation. It was also assumed that each of the look events by any of the satellites in the constellation was successful for calibration. The time elapsed between each of these look events was used to calculate r_ε, as shown in Eq. 10. These results were then used to compute EDA$_{adj}$ (based on Eq. 11), and the results are shown in Fig. 5.

In this particular case (shown in Fig. 4), the EDA$_{adj}$ is 2912.80 Terabytes (TB) for a = 0, and it

declines to 2386.54 TB for a = 0.25%, and to 1636.73 TB for a = 1%. These results represent a conservative estimate (due to the simplifying assumptions) and due to the coarse grid discretization used for the orbital simulation.

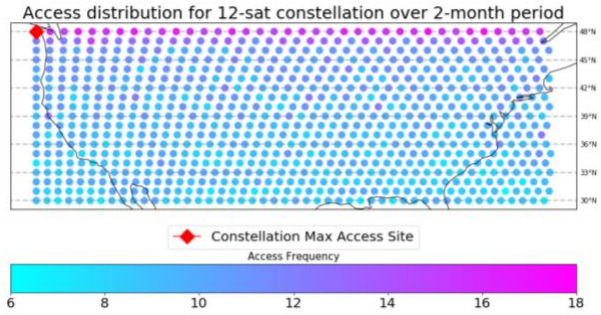

Figure 3: Points of Interest generated by architecture within a Region of Interest (CONUS). The color corresponds to access times by constellation. The red diamond corresponds to the site with the highest number of constellation access.

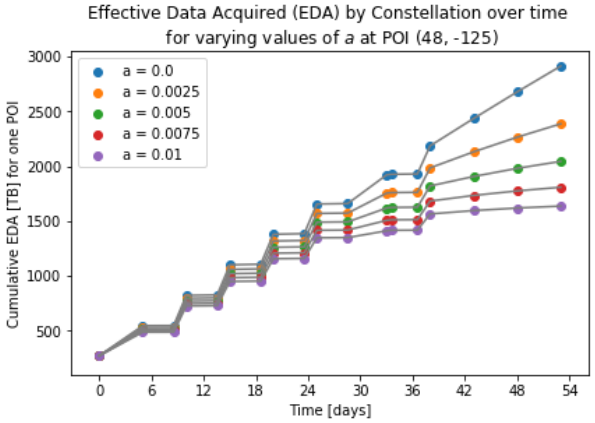

Figure 4: EDA over time for the constellation max access site, with varying values of a. Note that the last constellation access is on day 54, while the simulation runs for 2 months.

Overall, this case demonstrates an initial proof-of-concept application of the method, and shows that with larger values of a (*i.e.* with faster degradation), the EDA_{adj} declines over the course of the mission as compared to what it would be if there was no degradation (case of a = 0).

This approach (with higher fidelity simulations) can be used for relative comparisons of key design parameters for new constellation architectures, choice of calibration site locations, and frequency of calibration. Conversely, it can also be used for assessing utility of calibration sites and calibration frequency for deployed systems with specific orbital geometrics and coverage characteristics.

Case B: Quantifying impact of calibration with difference in constellation EDA

The second application case analyzed a constellation deployed for global observation. In this case, a 4-satellite constellation with identical instrument specifications as in Case A was modeled, and simulated for a 90-day period. It was also assumed, for simplicity of logistics, that terrestrial calibration sites are to be located below the Arctic Circle (latitudes of 66.5° or lower).

Figure 5 shows the results of the simulation. Four sites, below 66.5° latitude were identified to have the highest access frequency (marked in red, blue, green and yellow), and the site in black diamond was assumed to be the calibration site. This site (located at 65.7303, -150.411 near Fairbanks, Alaska and accessed 13 times over 90-days) had a weekly re-visit on average.

The EDA for varying values of a was computed, and the results are shown in Figure 6. Figure 6 shows both the case with satellite calibration (6b), and without satellite calibration (6a). As can be seen in Figure 6a, sensor degradation with varying values of a result in loss of EDA. This is offset by calibration in Fig. 6b. Figure 7 shows the per-satellite cumulative EDA for the same calibration site. Given the SSO inclination of the constellation, satellite orbits precess over time, explaining how the POI appears within the view of satellite 0, 2, and 3, and then leave after a certain period of time.

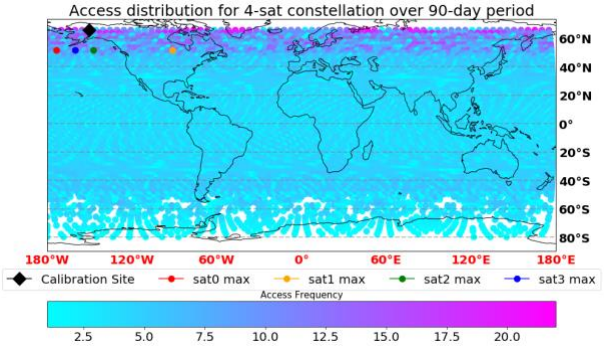

Figure 5: Points of Interest within a global Region of Interest (ROI), with the constraint of latitudes < 66.5 °. The color corresponds to access frequency by constellation. The dots with labels are the points associated with maximum access by each of the satellites. The black diamond was chosen as the calibration site for the constellation.

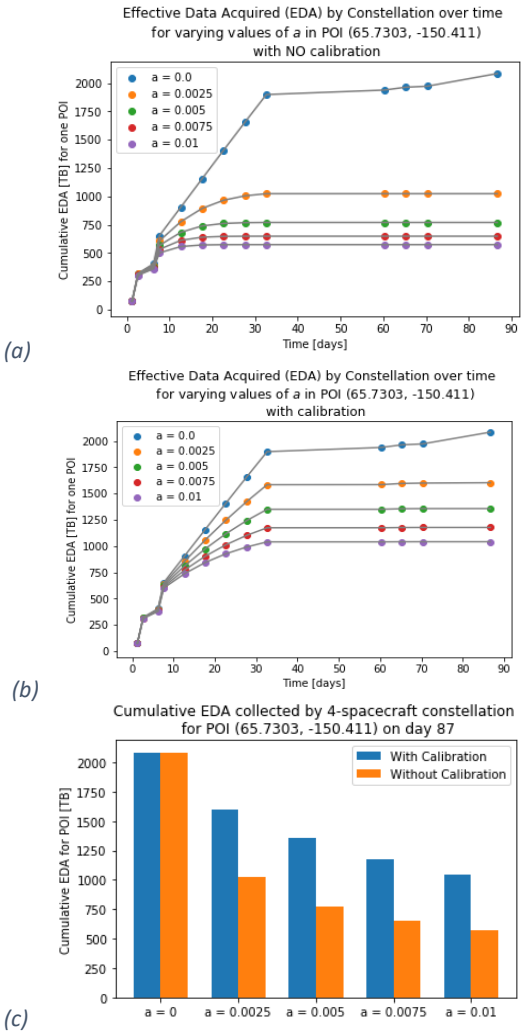

Figure 6: EDA for one Point of Interest (POI) for the constellation. 6a shows the case without calibration, and 6b is the case with calibration. 6c compares the cumulative EDA collected by day 87, for both the calibration (blue) and no-calibration (orange) case.

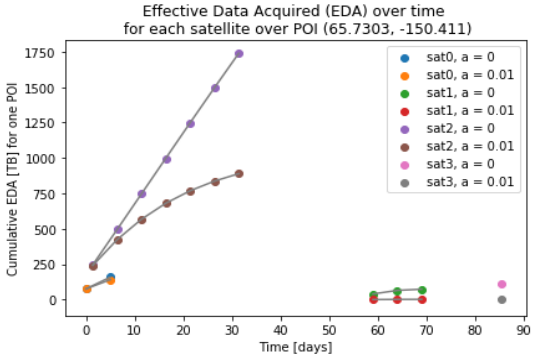

Figure 7: Cumulative EDA for one POI for each of the 4 satellites, with a = 0, for no sensor degradation over time and a = 0.01, an extreme case of sensor degradation of 1 % / day.

SUMMARY, LIMITATIONS, AND FUTURE WORK

This paper shows how calibration can be integrated in a general valuation framework, through the inclusion of time-based factors that capture data degradation between intervals of calibration. Such an adjusted (or discounted) value quantification method allows for a systematic and theoretically-grounded basis for obtaining data value with sensor calibration.

This paper has developed a model and demonstrated a proof-of-concept application for a pre-phase A level analysis. There is further work required to refine the discounting parameters, and to rigorously link them with empirical data. Several studies have characterized calibration stability of VIS, NIR and SWIR spectral bands over multiple years [24–26] for SeaWiFS, ALI, Terra and Aqua MODIS, and Landsat's OLI instruments. However, empirical data for passive imaging sensors on small spacecraft is not readily available, and the accumulated experience with imaging sensors on small satellites is not as extensive.

There are also limitations in the orbital simulations in this work. One of the major assumptions made is the existence of only one calibration site for the constellation–likely, there will be several calibration sites available for each satellite, however these may require scheduling with other satellite overpasses. Future work will examine the look opportunities for each satellite across several calibration sites, and the impact on the EDA_{adj}. Another key assumption is on counting every look opportunity as a successful calibration event. In practice, calibration opportunities are constrained by factors such as meteorological events (such as cloud cover). These were not factored in this work.

As a tool for projects in pre-phase A, TAT-C limits POI generation, and less than 10,000 POI were used for a global simulation. For large Regions of Interest (such as the whole planet), there may be areas that present as suitable calibration sites but are not analyzed in the simulation. In identifying suitable locations for calibration sites, higher granularity will be needed. The choice of constellations will also be subject of further work. While the analysis was done for two constellations of differing numbers of satellites, both constellations employed SSO inclination. SSO inclinations precess over time and exhibit higher access events in the higher latitudes, as can be seen in both Figure 5 and Figure 3. The locations of calibration sites will differ for missions with different orbital parameters.

Another important limitation in this work is the simplification of monetary parameters, such as monetary value of per unit data (defined with the parameter ω), and

exclusion of system costs. For a full accounting of value, both costs and benefits (accrued with data sales at some price) have to be modeled and evaluated. In future work, the limitations discussed above will be addressed with further data collection and modeling. In particular cost modeling and data price modeling will be developed and explicitly included.

Further methodological additions will also be made. In this paper, the focus was on the technical data acquisition and calibration processes that are only part of a larger data value chain, wherein data is acquired, transmitted, processed, and reduced into specific forms such that it can be used for human decisions and actions. In this chain of data processing, the role of algorithms, machine learning, and other emerging methods are salient, wherein efforts are being made to improve analysis, inference, and decision making. Additionally, in this work, the time-related discounting of value focused only on the temporal data degradation aspects. There are, however, other systems-level considerations that can also be made regarding the discounted time-value of data. For some applications, the timely acquisition, processing, delivery, and use in decision-making drives its value. Examples of such cases include data acquisition for weather forecasts, tracking hurricanes, floods, or wildfires. For such cases, the data embeds time-sensitive information that can inform time-sensitive decisions, and consequently impact safety of human lives and protection of property and built infrastructure. In such cases the full data value chain (from acquisition to decisions to action) needs to be considered to fully characterize the time-related value of data.

In on-going work, the authors are developing methods to quantify the errors and uncertainties that accumulate and propagate in data value chains of remote sensing systems, and using those errors to assess the value of data for different applications [3]. In future work, those methods will be linked with the approach presented here that will allow for investigating important questions related to not only optimizing system architecture and technical design, but also connecting with questions of data accuracy and value delivery.

Lastly, and importantly, when considering *value delivery* [27], a key question to ask is: "value for who?" For many EO systems, the value for the public (or societal value) is of interest for applications that serve public needs. But value for system operators, data providers, and subscribers (of different data products) also needs to be duly understood to guide planning, design, and operations of new earth observation systems. In future work, these questions will be explored in greater depth.

Acknowledgments

We thank Eric Magliarditi for assisting with implementing software for computing Effective Data Acquired (EDA) over time using simulations of spacecraft constellations, and for providing helpful guidance with the Tradespace Analysis Tool for Constellations (TAT-C).

References

1. Bouvet, M. *et al.* RadCalNet: A radiometric calibration network for earth observing imagers operating in the visible to shortwave infrared spectral range. *Remote Sens.* **11**, (2019).

2. NIST. *Achieving Satellite Instrument Calibration for Climate Change - ASIC3*. (2007). doi:10.1017/CBO9781107415324.004

3. Siddiqi, A., Baber, S., de Weck, O. . & Durell, C. Error and Uncertainty in Earth Observation Data Value Chains. in *International Geoscience and Remote Sensing Symposium (IGARSS)* (IEEE, 2020).

4. Siddiqi, A., Magliarditi, E. & de Weck, O. L. Valuing New Earth Observation Missions for System Architecture Trade-studies. in *IEEE International Geoscience and Remote Sensing Symposium* 1–4 (2019).

5. LeMoigne, J. *et al.* End-to-End Trade-space Analysis for Designing Constellation Missions. in *AGU Fall Meeting Abstracts* (2017).

6. Foreman, V., Siddiqi, A. & de Weck, O. L. Advantages and Limitations of Small Satellites in Low Earth Orbit Constellations: A Prospective Review. in *Small Satellite Conference* (2018).

7. NRC. *The Role of Small Satellites in NASA and NOAA Earth Observation Programs*. (2000). doi:https://doi.org/10.17226/9819

8. Millan, R. M. *et al.* Small satellites for space science: A COSPAR scientific roadmap. *Adv. Sp. Res.* **64**, 1466–1517 (2019).

9. USGS. LandSat 8 Calibration. Available at:

https://www.usgs.gov/land-resources/nli/landsat/landsat-8-oli-and-tirs-calibration-notices.

10. Helder, D. L. *et al.* Radiometric calibration of the landsat MSS sensor series. *IEEE Trans. Geosci. Remote Sens.* **50**, 2380–2399 (2012).

11. GSFC. Landsat 8 Overview. Available at: https://landsat.gsfc.nasa.gov/landsat-8/landsat-8-overview/. (Accessed: 6th October 2019)

12. Reising, S. C. *et al.* Temporal Experiment for Storms and Tropical Systems Technology Demonstration (TEMPEST-D): Reducing risk for 6U-Class nanosatellite constellations. *Int. Geosci. Remote Sens. Symp.* **2016-Novem**, 5559–5560 (2016).

13. Chander, G. *et al.* Overview of intercalibration of satellite instruments. *IEEE Trans. Geosci. Remote Sens.* **51**, 1056–1080 (2013).

14. Houborg, R. & McCabe, M. F. Daily retrieval of NDVI and LAI at 3 m resolution via the fusion of CubeSat, Landsat, and MODIS data. *Remote Sens.* **10**, (2018).

15. McCabe, M. F., Aragon, B., Houborg, R. & Mascaro, J. CubeSats in Hydrology: Ultra high-Resolution Insights Into Vegetation Dynamics and Terrestrial Evaporation. *Water Resour. Res.* **53**, 1–8 (2017).

16. Geng, F., Saleh, J. H., Tien, A. & Herd, R. A. Beyond Cost Tools : Spacecraft Net Present Value and the Hosted Payload Paradigm. *IEEE Trans. Aerosp. Electron. Syst.* **51**, 3348–3363 (2015).

17. Wertz, J. R. & Larson, W. J. *Space Mission Analysis and Design*. (Microcosm Press, 1999).

18. Magliarditi, E., Siddiqi, A. & Weck, O. De. Remote Sensing for Assessing Natural Capital in Inclusive Wealth of Nations : Current Capabilities and Gaps. in *IEEE International Geoscience and Remote Sensing Symposium* 4411–4414 (2019).

19. Mather, P. M. & Koch, M. *Computer Processing of Remotely-Sensed Images: An Introduction*. (Wiley, 2011).

20. Wolfram-Continuous and Discrete time discounting. Available at: https://demonstrations.wolfram.com/ContinuousAndDiscreteTimeDiscounting/.

21. Johnstone, D. Sensitivity of the discount rate to the expected payoff in project valuation. *Decis. Anal.* **14**, 126–136 (2017).

22. Le Moigne, J. *et al.* Tradespace analysis tool for designing constellations (TAT-C). *Int. Geosci. Remote Sens. Symp.* **2017-July**, 1181–1184 (2017).

23. Ravindra, V. Instrument Data Metrics Evaluator for Tradespace Analysis of Earth Observing Constellations. (2020).

24. Xiong, X. & Butler, J. Challenges and Approaches for Sensor Reflective Solar Calibration. in *International Geoscience and Remote Sensing Symposium (IGARSS)* 5796–5799 (IEEE, 2019). doi:10.1109/IGARSS.2019.8899022

25. Wu, A. *et al.* Characterization of Terra and Aqua MODIS Calibration Stability. *IEEE Trans. Geosci. Remote Sens.* **51**, 4330–4338 (2013).

26. Kieffer, H. H. *et al.* On-orbit radiometric calibration over time and between spacecraft using the Moon. in *SPIE Proceedings International Symposium on Remote Sensing* **4881**, 287 (2002).

27. Crawley, E., Cameron, B. & Selva, D. *System Architecture: Strategy and Product Development for Complex Systems*. (Pearson Higher Education, 2016).